Meteoritics & Planetary Science 37, 407–420 (2002)
Available online at http://www.uark.edu/meteor

Space shuttle observations of terrestrial impact structures using SIR-C and X-SAR radars

JOHN F. MCHONE[1]*, RONALD GREELEY[1], KEVIN K. WILLIAMS[1], DAN G. BLUMBERG[2] AND RUSLAN O. KUZMIN[3]

[1]Department of Geological Sciences, Box 871404, Arizona State University, Tempe, Arizona 85287-1404, USA
[2]Department of Geography and Environmental Development, Ben-Gurion University of the Negev, P.O. Box 653, Beer Sheva 84105, Israel
[3]Vernadsky Institute, Russian Academy of Sciences, Kosygin Street 19, Moscow 117975, GSP-1 Russia
*Correspondence author's e-mail address: jmchone@hotmail.com

(Received 2001 May 31; accepted in revised form 2001 December 6)

Abstract–Ten terrestrial impact structures were imaged during two flights of the 1994 space radar laboratory (SRL) experiment. These craters include Wolf Creek, Australia; Roter Kamm, Namibia; Zhamanshin, Kazakhstan; BP and Oasis, Libya; Aorounga, Chad; Amguid, Algeria; and Spider, Connolly Basin and Henbury, Australia. SRL contained two co-registered instruments; the United States shuttle imaging radar-C (SIR-C) polarimetric radar system operating in L-band (λ = 24 cm) and C-band (λ = 5.6 cm), and the joint German/Italian synthetic aperture radar (X-SAR) operating in vertically-polarized X-band (λ = 3 cm).

Comparisons show SRL images to be complementary to, or in some cases superior to, corresponding optical images for evaluating size, location, and relative age of impact features. Regardless of wavelength or polarization, craters with significant relief appear prominently on radar as a result of slope and roughness effects. In desert regions, longer wavelengths penetrate dry sand mantles to reveal hidden crater dimensions or associated buried landforms. Radar polarities and wavelengths are particularly sensitive to vegetation, surface roughness, and soil moisture or electrical properties. In the more temperate environments of Kazakhstan and Australia, SRL images show detailed stream patterns that reveal the location and structure of otherwise obscured impact features.

INTRODUCTION

Approximately 170 impact craters or their ancient and eroded remnants, termed astroblemes, are now known or suspected on Earth (Grieve and Shoemaker, 1994; Grieve *et al.*, 1995; Hodge, 1994). Three of these features, Wolf Creek in Australia, Roter Kamm in Namibia, and Zhamanshin in Kazakhstan, were targeted for data acquisition by the space radar laboratory (SRL) which orbited Earth in April (SRL-1) and October (SRL-2) of 1994 onboard two space shuttle missions (STS-59 and STS-68). All three impact structures were imaged successfully with multiple passes and look directions. In addition, several other impact sites were fortuitously imaged while radar data were being collected for other purposes. These additional locations include four sites in hyper-arid Africa: the BP and Oasis structures in Libya, the Aorounga structure in Chad, and Amguid crater in Algeria; and three sites in semi-arid Australia: the Spider and the Connolly Basin astroblemes and Henbury crater field.

The SRL system obtained digital radar data in three wavelengths (λ): L-band (λ = 24 cm), C-band (λ = 5.6 cm), and X-band (λ = 3 cm) (Stofan *et al.*, 1995; Jordan *et al.*, 1995). L- and C-band systems could transmit and receive in horizontally (H) or vertically (V) polarized modes, providing the complete scattering matrix of HH, HV, VH, and VV combinations. The X-band system operated in a VV polarization. These multiple wavelengths and polarizations, combined with the opportunity during the mission to target sites repeatedly with different viewing geometries and incidence angles (Table 1), provide the opportunity to assess the utility of radar for a wide variety of scientific investigations.

In this report, we discuss the characteristics of several known terrestrial impact structures as viewed by SRL and compare our results with optical images and previous studies. All radar images used in this study were processed and examined at a nominal resolution of 25 m. The purpose is to determine if radar data either reveal previously unknown aspects of impact craters or fail to reveal features discernible in conventional aerial or orbital photographs.

PRE-SELECTED IMPACT CRATERS

Wolf Creek and Rotor Kamm craters were selected for their conventional, simple bowl shaped morphologies emplaced in

TABLE 1. Shuttle radar laboratory data for impact features.

Crater	Diameter (km)	SIR-C Data-take	Mode*	Mission	Incidence angle (°)	Look†
Amguid	0.45	109.00	8	2	54.7	RA
Aorounga	12.6	140.10	11	1	31.9	RA
		124.00	16	1	23.3	RA
BP	3.2	060.10	8	2	26.7	LA
Connolly	9.0	117.51	8	2	47.2	RA
Henbury	0.006–0.15	021.80	16	2	30.7	RA
Oasis	>17.0	108.10	11	2	36.0	RA
Roter Kamm	2.5	074.80	11	1	48.1	RA
		036.80	11	2	23.5	RD
Spider	11–13	031.50	11	1	56.2	LD
Wolf Creek	0.875	149.41	16	1	40.6	LA
		031.50	11	1	56.1	LD
Zhamanshin	14.0	079.30	11	1	50.6	RD
		028.30	11	1	52.5	RA
		111.30	16	1	44.5	RD
		127.40	9	1	41.9	RD
		095.60	11	1	47.9	RD

Mode*	Transmit	Receive	Look†
11	H	HV	R = Right
16	HV	HV	L = Left
9	V	V	A = Ascending orbit
8	H	H	D = Descending orbit

active aeolian environments. Zhamanshin was chosen for its more complex structure and its high-latitude location that placed it repeatedly within range of the space shuttle inclined orbit.

Wolf Creek Crater, Australia

Wolf Creek, also known as Wolfe Creek, is an 875 m diameter impact crater located at 19°10' S, 127°47' E on the eastern margin of the Great Sandy Desert, Western Australia (Fig. 1). The crater was first identified by Reeves and colleagues from an aircraft and later confirmed as an impact structure with associated iron meteorites (Reeves and Chalmers, 1949). The crater is 50 m deep and has a diameter of 870 to 950 m (rim to rim), giving a depth-to-diameter ratio of 1:19. The rim rises 25–35 m above the surrounding surface. The crater lies in Devonian sandstones and Neogene laterites and is floored with aeolian sediments and secondary gypsum deposits. Berylium and chlorine isotope abundances in the iron meteorite indicate an impact age of ~300 000 years (Shoemaker *et al.*, 1990).

SRL radar images of Wolf Creek crater (Fig. 2) show a bright outer ring and a bright central feature corresponding to the rim and the crater floor. High radar backscatter from the floor is attributed to vegetation, sinkholes, and gypsum deposits. A radar-mottled zone surrounding the bright central feature corresponds to sands trapped within the crater. On aerial photography (Fig. 1), the west rim of the crater appears to be wider than the east rim, where it is partly mantled by sand. On the L-band radar image (Fig. 2a), the rim appears to be of more uniform width, possibly because radar energy penetrating a thin sand mantle is returned from rocks comprising the rim. In addition, the radar image shows a slight widening of the rim on the southwest side of the crater. This area is characterized by greater fracturing, which produces slightly stronger

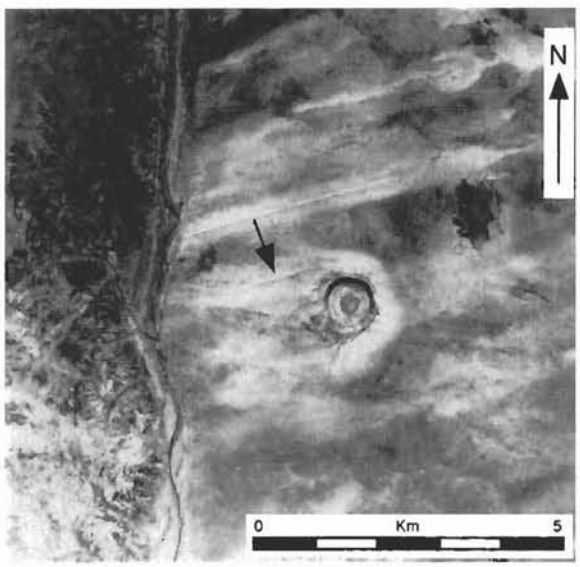

FIG. 1. Aerial photograph of Wolf Creek impact crater, Australia. High albedo collar surrounding the crater corresponds to sand sheets and small duneforms developed by the predominantly westward (toward the left) winds. Dark spot in the center of the crater represents vegetation. Arrow marks sand ridge (linear dune). Area shown is 9.4 × 9 km (ASU photograph 4226-H, original courtesy of R. S. Dietz).

radar backscatter. This asymmetric character of the rim is attributed to an impacting meteoroid arriving in a low-angle trajectory from the northeast (Guppy and Matheson, 1950).

Wolf Creek crater forms a topographic obstacle to regional winds flowing toward the west, and windblown sediments are distributed in distinctive patterns of sand erosion and deposition (*e.g.*, McCall, 1965). Sand deposits are visible on the aerial photograph as high albedo patches and streaks trending toward the west-southwest. A horseshoe-shaped collar of mobile sand wraps around the rim of the crater and forms two arms trailing leeward from the crater flanks. These patterns are similar to those seen on Mars (Greeley *et al.*, 1974) and Venus (Greeley *et al.*, 1992, 1994). The northern arm forms a dominant sand ridge. For the most part, the sand streaks are not visible on the radar images (Fig. 2), but the horseshoe-shaped collar of sand immediately southwest of the crater appears as a bright patch in the X-band image (Fig. 2b). This radar bright area could be due to small-scale sand ripples on the surface. A radar-bright, linear feature west of the crater in the X-band image may also be due to ripples, cobbles, or vegetation. It is worth noting that most sand dune crests in the area are oriented along an azimuth of 75°, or within 19° of the SRL look direction. As a result, much of the radar energy is reflected away from the spacecraft, thus curtailing dune visibility on the radar images. In addition, L-band energy can penetrate dry sand and render the streaks less visible. In contrast to the visibility of aeolian features, fluvial patterns west of the crater, which are of meter-scale roughness and larger, are more clearly defined in the L-band image (Fig. 2a) than in smaller wavelength images (Fig. 2b).

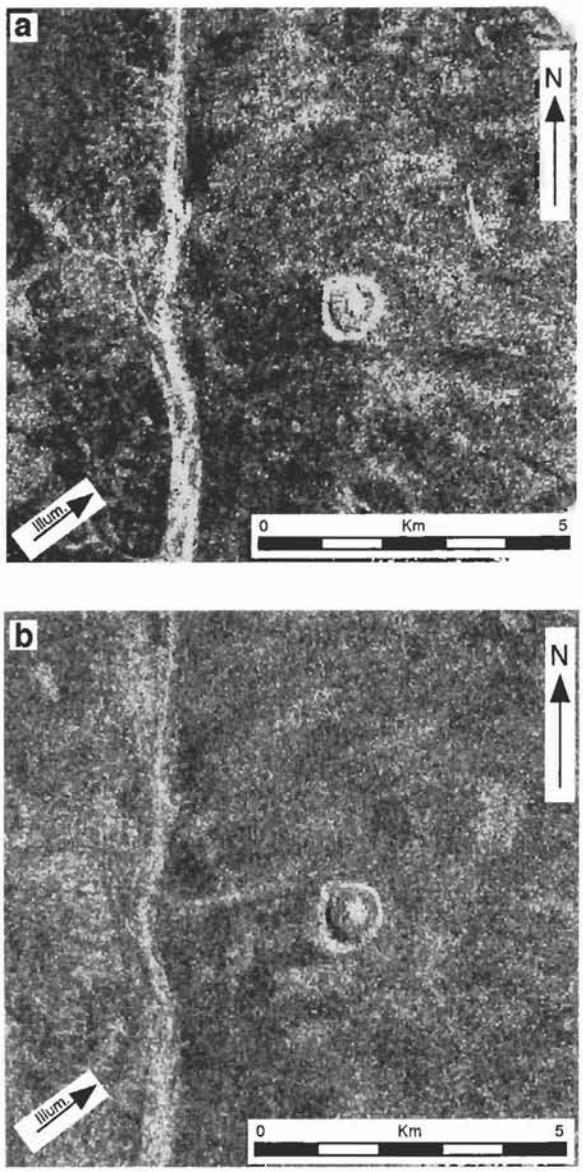

FIG. 2. SRL images (DT-31.05) of Wolf Creek impact crater in (a) L-band HH (ASU photograph IPF-1002) and (b) X-band VV (ASU photograph IPF-984).

Roter Kamm Crater, Namibia

Roter Kamm is a bowl-shaped impact crater ~2.5 km in diameter, located in the western Namib Desert of Namibia at 27°46' S, 16°18' E (Fig. 3). Dietz (1965) first proposed an impact origin based on morphology. The site was later confirmed as an impact crater based on the discovery of impact breccia, microscopic shock metamorphic features, and radial joint patterns (Fudali, 1973; Miller and Reimold, 1986; Reimold and Miller, 1989). Its age is estimated to be 3.4 to 4 Ma (Koeberl *et al.*, 1993).

Roter Kamm is a very shallow, circular structure with a narrow raised rim formed in Precambrian granites and

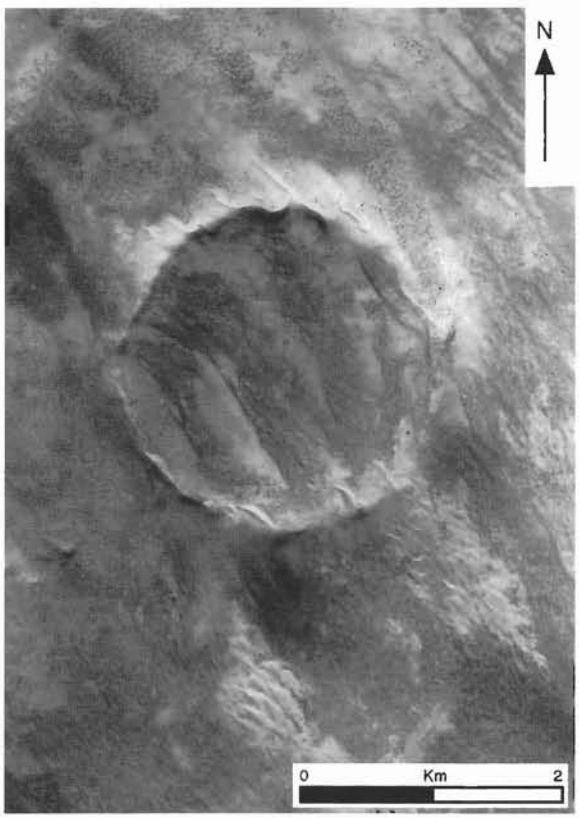

FIG. 3. Aerial photograph of Roter Kamm impact crater, Namibia, showing rim and superimposed sand sheet and dune deposits. Prevailing winds are toward the northwest (upper left of photograph). Area shown is 6 × 4.3 km (ASU photograph 4227-H, original courtesy of R. S. Dietz).

metamorphics. The crater is partly mantled by active sand deposits. Linear dunes form short (<700 m) streaks that are visible on aerial photographs and radar images (Figs. 3 and 4). Also visible on radar images is a halo zone of moderate backscatter, which extends ~1 km from the crater rim. Bomb-shaped breccias occur on the rim (Reimold *et al.*, 1988), suggesting that ejecta and other impact-fragmented materials are present. Although the terrain around the crater rim is mantled with sand, the halo could represent blocks of ejecta that reflect radar energy that penetrated the sand mantle. At a steeper incidence angle (Table 1), the linear dunes and the halo zone around the crater appear less distinct but wind streaks become more prominent, especially in the area north of the crater. In general, large surface roughness (such as dunes a few meters tall) is better depicted with shallow incidence angles (incidence angle <25°). In contrast, surface roughness at the submeter scale is better differentiated at incidence angles steeper than 35° (Elachi *et al.*, 1982).

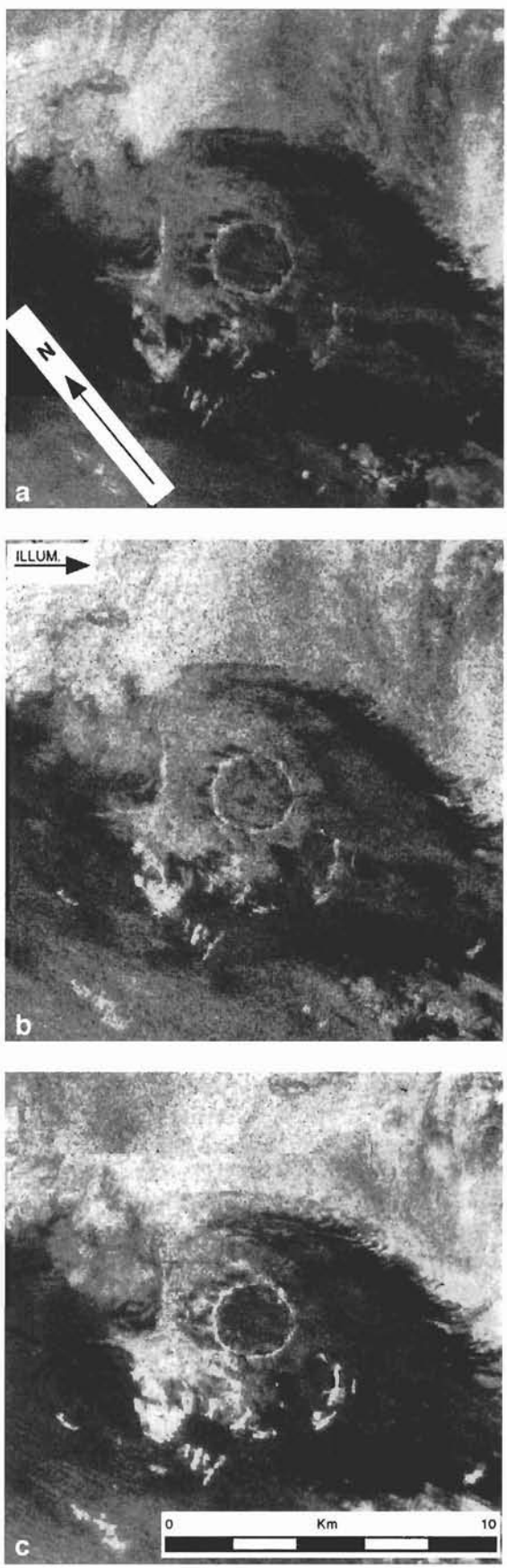

FIG. 4. *(right)* SRL images (DT-74.80) of Roter Kamm impact crater in (a) X-band VV, (b) C-band HH, and (c) L-band HH (ASU photograph IPF-987).

Zhamanshin Impact Crater, Kazakhstan

Zhamanshin is a 14 km diameter impact structure (Florensky and Dabizha, 1980), located in Kazakhstan at 48°22' N, 60°58' E. As described by Masaitis *et al.* (1984) and Garvin and Schnetzler (1994), the structure includes a topographic inner ring that is ~6 km across. Zhamanshin formed in flat-lying Eocene and Oligocene sedimentary rocks overlying Paleozoic and Mesozoic metamorphic rocks. The crater has been deeply eroded and partly filled with Quaternary loess and lacustrine deposits. The eastern side is breached by fluvial erosion.

SRL data were acquired on five data takes (Table 1). In X-band, the craterform is very difficult to identify because vegetation, cobbles, and small-scale roughness produce a strong radar backscatter for the entire area. The structure is somewhat better seen in C-band, but the numerous gullies also result in a strong ground-clutter signal. In contrast, the longer wavelength L-band clearly highlights distinct stream channels with distribution patterns controlled by the craterform (Fig. 5).

Figure 6a is a geological sketch map adapted from Masaitis *et al.* (1984), showing the inner and outer rings, and the proposed extent of ejecta. Also shown are 1–2 order and 3–5 order streams, as identified on the L-band image. The 1–2 order streams are 1–2 m wide and are particularly prominent on the image because the gully walls produce strong backscatter. Figure 6b shows the frequency distribution of 1–2 order streams. A zone of highest stream density corresponds to the inward-facing slope of the outer ring, and to the outward-facing flanks of the crater. A broad loop of moderately low stream density (0.8–1.2 km^{-2}) corresponds to the level planar surface immediately surrounding the outer ring.

Although stream patterns tend to outline the presence of a subtle craterform, it is unlikely that the Zhamanshin structure would have been identified from radar images alone.

FIG. 5. SRL L-band VV image (DT-127.40) of the Zhamanshin feature, Kazakhstan, corresponding to the sketch map shown in Fig. 6a (ASU photograph IPF-977).

ADDITIONAL IMPACT SITES ACQUIRED IN HYPER-ARID AFRICA

The four African sites fortuitously imaged by SRL are characterized by a nearly total lack of near-surface soil moisture. Their distinct appearances reflect the ability of radar to penetrate dry sediments to a depth of several wavelengths.

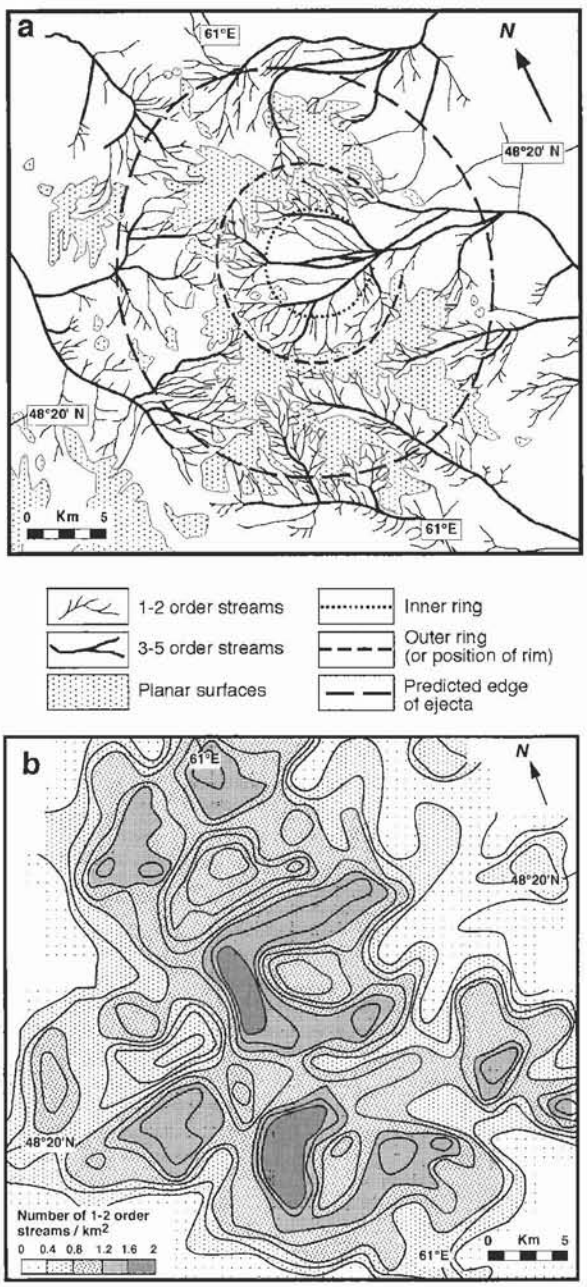

FIG. 6. (a) Geologic sketch map of the Zhamanshin feature adapted from Masaitis *et al.* (1984) and showing stream patterns mapped from the SRL image (Fig. 5). (b) Map showing densities of first- and second-order streams per square kilometer; high densities correspond to gullies developed on the inner wall and the outer flank of the crater form.

BP Structure, Libya

The BP structure (a name derived from the initials for British Petroleum) is located in the Libyan Desert at 25°19' N, 24°20' E, ~165 km northeast of Kufra Oasis. It is a 3.2 km diameter crater formed in Nubian Sandstones of early Cretaceous age (French *et al.*, 1974). The BP structure was first recognized by Martin (1969) and has been dated only as younger than the target rocks, or <127 Ma (Underwood, 1976). Aerial photographs (Fig. 7) show a prominent inner ring and an outer ring composed of concentric, discontinuous ridges. The center of the structure is marked by a central peak some 15 m high. Windblown sands mantle much of the crater and make it difficult to study on low-resolution optical images.

On the SRL L- and X-band images (Fig. 8), the central uplift and the inner and outer rings of deformed rock are clearly seen. Comparison with the aerial photograph (Fig. 7) suggests that radar energy penetrates the shallow sand mantle to reveal a nearly complete "bulls-eye" pattern typical of impact structures with central uplifts. The concentric pattern is further enhanced by low radar backscatter which corresponds to thicker sand deposits on the crater floor and between the deformed rocks.

Although previous estimates of the crater diameter placed it at 2.8 km (Martin, 1969), SRL images show that the impact structure has a maximum diameter of at least 3.2 km. In addition to a larger size, radar images reveal a subtle subsurface drainage pattern surrounding the outer rim that is poorly seen on aerial and satellite optical images (Fig. 8a). Buried streams in the Sahara were reported in earlier radar missions (McCauley *et al.*, 1982) and suggest former fluvial activity in this now arid terrain. A buried drainage pattern near BP Crater is influenced by the crater morphology, suggesting that the crater existed during an earlier time of free-flowing surface water.

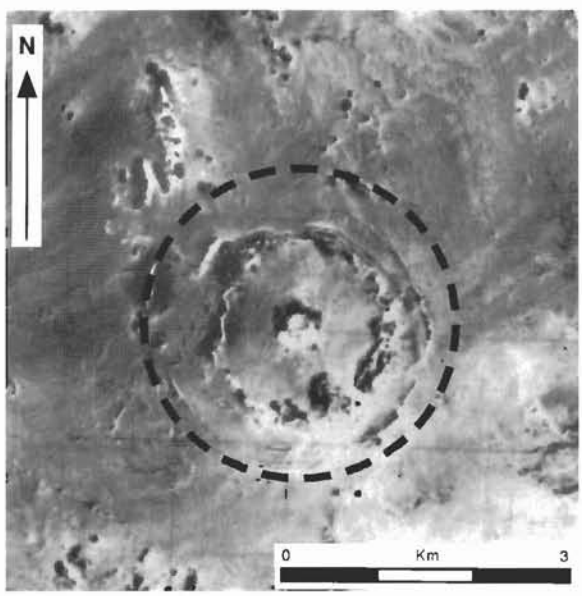

FIG. 7. Aerial photograph of BP structure, Libya, showing central uplift and concentric rings of deformed sandstone. High albedo areas are mantling deposits of sand. Dashed ring denotes a diameter of 3.2 km. Area shown is 5.5 × 6 km (ASU photograph 4228-H, courtesy of James R. Underwood).

Oasis Structure, Libya

The Oasis structure is located in Libya at 24°35' N, 24°24' E, ~80 km south of the BP structure (Fig. 9). Larger than 17 km in diameter, this structure was formed <127 Ma in the same

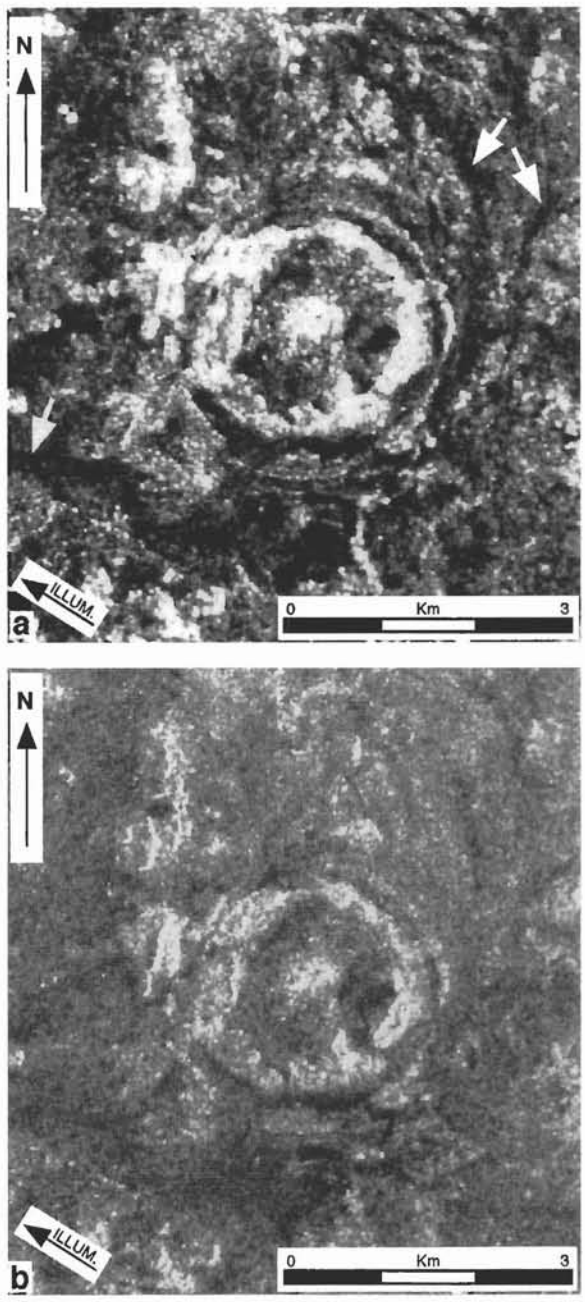

FIG. 8. SRL images of BP structure (a) L-band HH (DT-60.10; ASU photograph IPF-1007) and (b) X-band VV (DT-60.10; ASU photograph IPF-1009). Arrows in (a) indicate subtle buried drainage pattern evidently influenced by the crater morphology in a wetter climate.

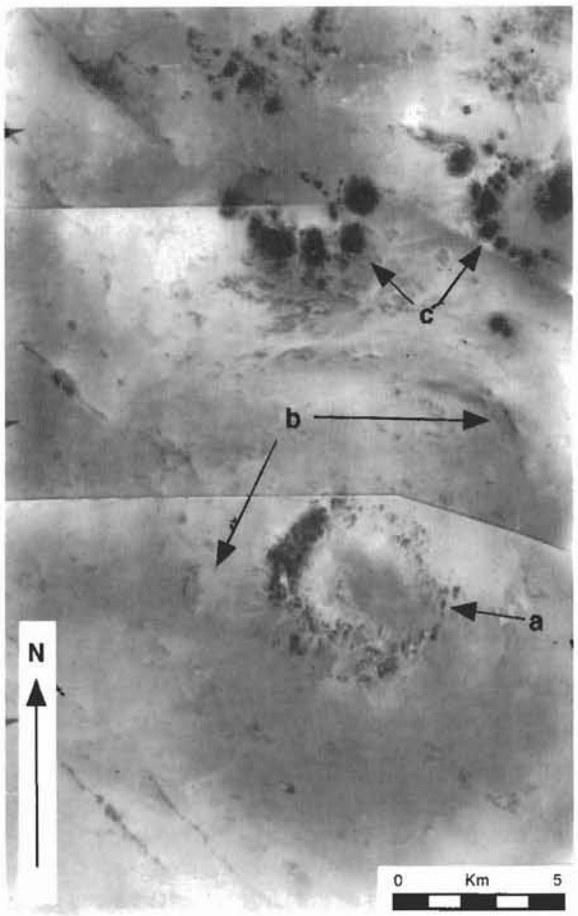

FIG. 9. Aerial photomosaic of the Oasis astrobleme, Libya showing the central ring of sandstone hills (a) surrounded by a sand-filled depression which is ~11 km in diameter. Subtle concentric patterns are shown by (b). Two partial rings visible to the north and northeast of the crater (c) are hills of dark, clastic sediments that were possibly emplaced as clastic plugs or "sand boils" during the impact event. Area shown is 28 × 17 km (ASU photograph 4231-H, courtesy of James R. Underwood).

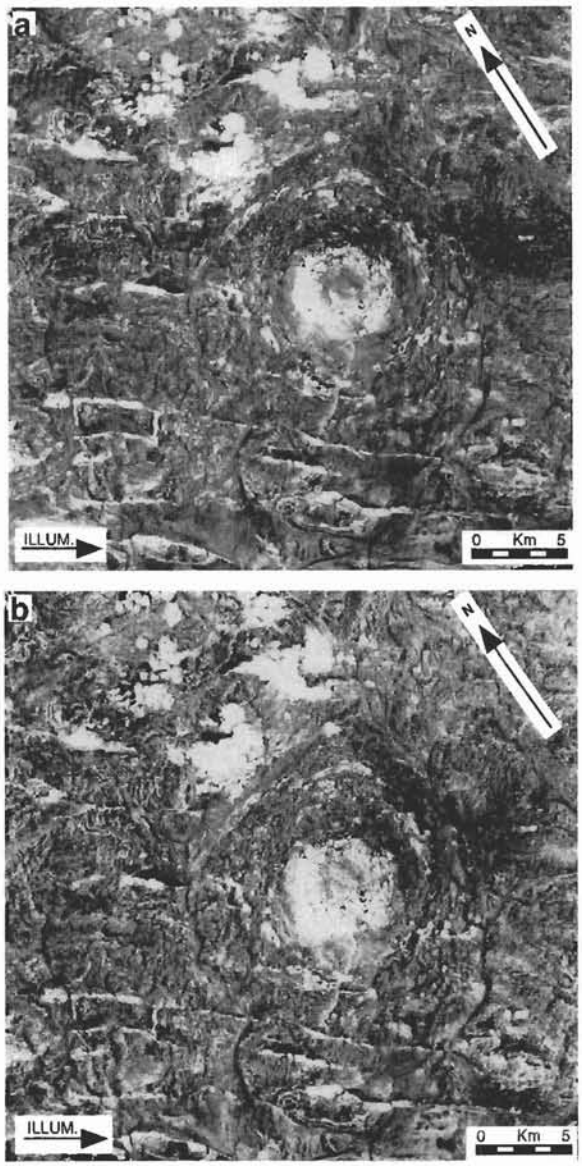

FIG. 10. SRL-1 images of Oasis astrobleme (a) L-band HH (DT-108.10) and (b) C-band HH (DT-108.10) showing increased detail of sand-mantled areas, including outer crater boundaries and buried stream patterns.

early Cretaceous Nubian Sandstones as, and possibly simultaneously with, the BP structure (Underwood, 1976).

Although original descriptions of the structure suggested a diameter of 5.1 km, satellite images in the visible spectrum show subtle concentric patterns more than 11 km across (Dietz and McHone, 1979; El-Baz and Bahay, 1982; Koeberl, 1994). More recently available SRL images (Fig. 10) show additional arcuate segments that are not visible on the satellite optical images and suggest a diameter larger than 17 km.

North and northeast of the Oasis structure is a field of rounded sandstone knobs 10 to 100 m in diameter and 10 to 50 m high. These have been interpreted as clastic plugs or "sand boils" composed of fluidized sediments, perhaps emplaced during the impact event (Underwood, 1976). Alternatively, the knobs could be eroded remnants of other partly buried impact structures, possibly reflecting the breakup of the impacting object before striking the surface. SRL images (Fig. 10) show the knobs as radar-bright features. Also shown is the bedrock structure below the sand mantle. There is no indication of circular patterns associated with the knobs, suggesting that they are not separate impacts.

Aorounga Structure, Chad

The Aorounga structure (Fig. 11) is located at 19°6' N, 19°15' E in the Borkou region of the Sahara Desert, northern Chad. This 17 km diameter feature has been mentioned in numerous remote sensing reports with speculation that it is of impact origin. However, because it lies near the large Tibesti Massif and southeast of the Emi Koussi volcanic field, many

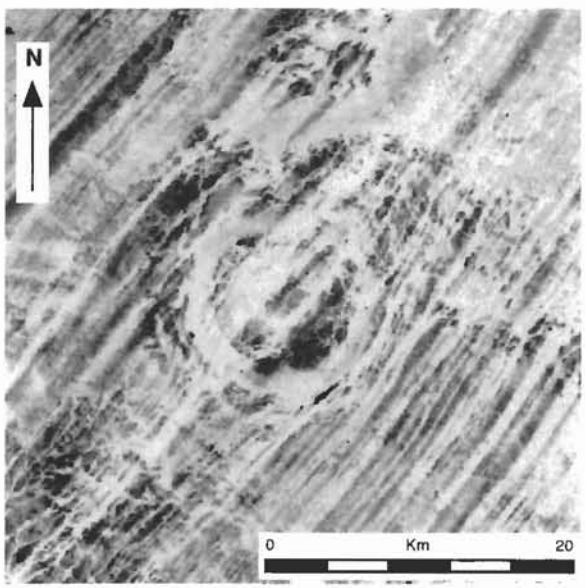

FIG. 11. Landsat 1, band 6 (0.7–0.8 μm) image of Aorounga structure, Chad. Bright albedo areas are sand deposits, and dark ridges are yardangs formed by northeasterly winds. Area shown is 30 × 30 km (Landsat frame E-1099-08831-6, ASU photograph 4229-H).

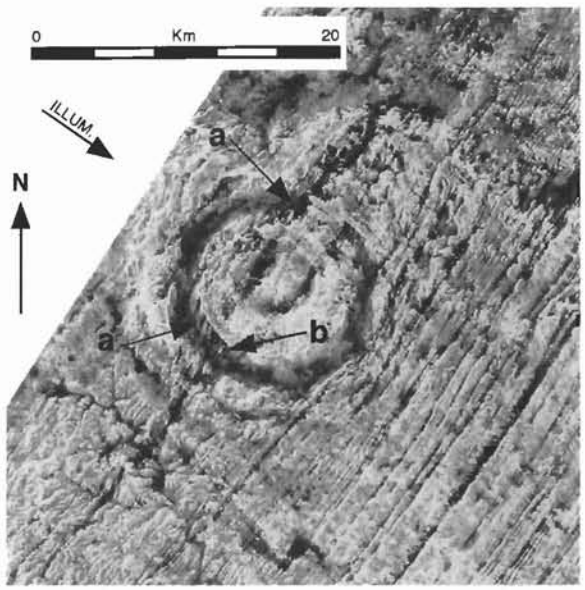

FIG. 12. SRL L-band HH image of Aorounga structure; arrows (a) indicate wind streaks formed by short linear dunes in the leeward slopes of the ring trough. Arrow (b) indicates bright star-like radar returns (SRL-1, DT 140.10; ASU photograph IPF-1006).

earlier investigators attributed it to a volcanic (Lowman *et al.*, 1966; Lowman, 1968; Lowman and Tiedeman, 1971; Grieve *et al.*, 1988) or plutonic (Roland, 1976) origin. More recent reports of shatter cones and shock metamorphic features revealed in petrographic studies strongly support an impact origin (Becq-Giraudon *et al.*, 1992; Grieve and Therriault, 1995; Koeberl *et al.*, 1998). Aorounga has not been dated but must be younger than the Upper Devonian sandstones in which it is formed (Koeberl, 1994).

Landsat images (Fig. 11) show Aorounga as a high albedo ring in a terrain of linear dark ridges tens of kilometers long separated by bright grooves, some of which are 0.3 to 1.5 km wide. The high albedo ring corresponds to a moatlike depression partly filled with windblown sand. Some of the ridges and grooves cut across the Aorounga structure. The dark ridges are well-known, wind-sculpted yardangs, and the bright grooves are intervening wind-cut valleys floored with sand deposits (McCauley *et al.*, 1977). The Borkou region of Chad is one of the windiest environments of the Sahara (Mainguet and Callot, 1978) and occupies a broad gap between the Tibesti Mountains to the northwest and the Ennedi Mountains to the southeast. Winds blow from the Libyan Desert though this gap for most of the year with stronger winter winds averaging 22 cm/s. The aeolian features reflect these primarily northeasterly winds.

Aorounga is very distinct in SRL images (Fig. 12) where it shows as a radar-dark ring. Low radar reflectivity within the ring is a result of trapped sand deposits which both absorb radar energy and also deflect it away from the spacecraft with their relatively smooth surfaces. Linear yardangs are particularly prominent because they are oriented nearly parallel to the spacecraft flight direction and orthogonal to the radar look direction, producing strong radar backscatter. Intervening topographic grooves are radar-dark, corresponding to the sand deposits. Trailing dunes have developed along several locations on the downwind slopes of the large trough ring and appear as radar-dark wind streaks (Fig. 12). The presence of well-organized chains of barchan dunes indicates a general paucity of granular sand. Tapering dune tails with sharp ridge crests which parallel the spacecraft flight direction have facets perpendicular to impinging radar and produce specular radar returns which appear as bright star-like spots.

Concentric ring segments southwest of the moat-like ring are visible on both the Landsat and SRL images and represent the outer limits of deformed crater rocks.

Amguid Crater, Algeria

Amguid crater is located in south-central Algeria at 26°5' N, 4°23' E. It is ~450 m in diameter and formed in plateau sandstones of Lower Devonian age that are moderately dissected by water-cut ravines and canyons (Fig. 13). The age of the impact is unknown, but based on its youthful state of preservation, it probably formed <100 000 years ago (Lambert *et al.*, 1980). Ejecta deposits are preserved, as described by Lefranc (1969) and Lambert *et al.* (1980). The floor of the crater contains playa deposits of fine-grained silts and clays. The crater is located on an elevated rocky highland and is identified on aerial photographs by the brilliant disk of high albedo playa deposits.

Amguid crater appears on SRL imagery (Fig. 14) as a thin, nearly complete circular ring of high radar backscatter

FIG. 13. Aerial photograph of Amguid crater, Algeria, showing prominent playa deposits on crater floor. Area shown is 3.5 × 4 km (ASU photograph 4230-H, courtesy of Inst. Geogr. Natl., Paris; photograph No. 575, Algeria sheet Aoulef 009-1952).

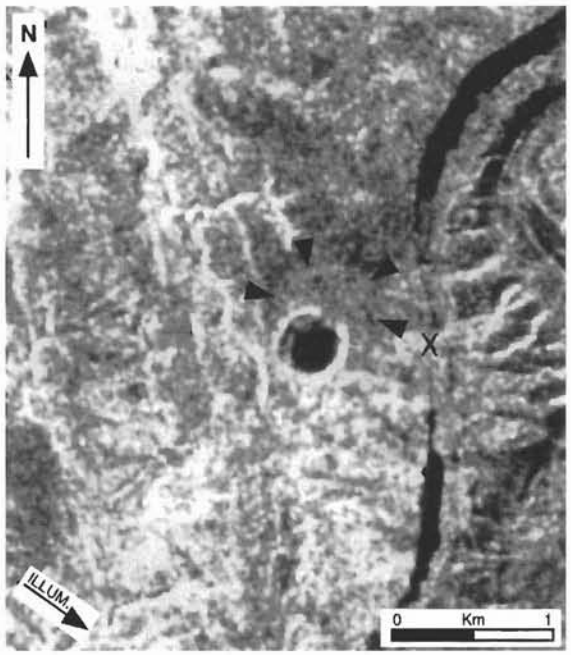

FIG. 14. SRL C-band HH image of Amguid crater. Very low radar backscatter corresponds to playa deposits on the crater floor, and arrows outline a possible lobe of ejecta. "X" marks the location of mass-wasted debris possibly triggered by the impact (SRL-1 DT-109.00; ASU photograph 4220-H).

corresponding to the steep inner wall and to uplifted and fractured rim rocks (Fig. 15). The very low radar backscatter on the crater floor corresponds to the fine-grained playa deposits (Fig. 16). A short discontinuity in the radar-bright ring on the north side marks a failed wall segment and its associated slump feature (Lambert *et al.*, 1980). Also apparent on radar are the ejecta deposits that appear as a coherent lobe attached to the north half of the crater. Landslide deposits outside the crater are visible in a canyon wall about one crater diameter east of the rim. Such deposits are rare in this region, and a landslide may have been triggered by the impact or developed later in rocks weakened by the cratering event.

ADDITIONAL IMPACT SITES ACQUIRED IN SEMI-ARID AUSTRALIA

In contrast to the African structures, the Australian impact sites in this study receive enough occasional rainfall to support a sparse cover of desert soils and vegetation. Radar is particularly sensitive to the presence of gravels and to the presence of grasses or scrub that develop in subtle patterns reflecting water runoff and soil moisture.

Spider Structure, Australia

The Spider astrobleme (16°44' S, 126°5' E) was recognized as an anomalous area of high relief (Fig. 17) during reconnaissance geologic mapping of the Kimberly Plateau in Western Australia (Roberts and Perry, 1970). Discovery of

FIG. 15. Photograph of the 50 m high wall on the west side of Amguid crater; rocky rim deposits and steep wall produce the high radar backscatter seen in Fig. 14 (photograph by J. F. McHone; ASU photograph 4219-D1).

deformed strata and shatter cones later confirmed an impact origin (Harms *et al.*, 1980) and prompted further detailed mapping (Shoemaker and Shoemaker, 1985, 1988, 1996). The structure is formed in early Proterozoic sandstones along the southern flank and near the hinge point and axis of the east-west-trending Mount Barnett Syncline (Fig. 18). Disrupted target rocks occur within a 13 × 11 km wide structural depression oriented along a northwest-southeast major axis. A central structural dome 0.5 km in diameter is mostly surrounded by a series of imbricated sandstone thrust sheets. These thin overlapping sandstone layers, exhumed by erosion, produce a pattern

FIG. 16. Photograph toward the north across Amguid crater, showing playa deposits on the crater floor and rock rim deposits (photograph by J. F. McHone; ASU photograph 4219-D8).

FIG. 17. Landsat 1, band 6 image (E-1378-01031-6) of the Spider structure, Australia (arrow). Area shown is 19 × 25 km (ASU photograph 4222H).

of radiating, topographic ridges that resemble "spider legs" in map view. Individual beds were thrust from the northwest to the southeast, suggesting that the bolide impacted on a low angle trajectory from the northwest (Shoemaker and Shoemaker, 1996).

SRL images (Fig. 19) of the Spider astrobleme show the structural depression as a radar-dark mottled area surrounding a radar-bright inner core corresponding to the thrust sheets and central dome. The darker outer trough corresponds to the smoother topography of sedimentary deposits which contrast with the more rugged inner highlands.

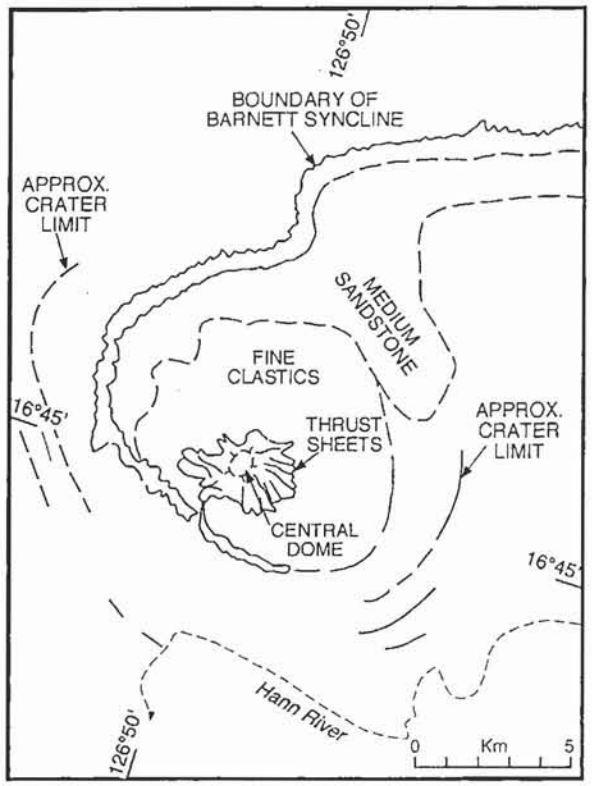

FIG. 18. Sketch map of the Spider structure showing general boundaries of the astrobleme and those elements that are visible in radar (Fig. 19). The outermost features as mapped by detailed fieldwork (E. M. Shoemaker, pers. comm., 1995) are not prominent on radar. However, the bright central dome, the bright splayed pattern of inner imbricated thrust sheets, and a darker halo of smoother sediments within the annular structural depression are all recognizable units in the radar images.

Connolly Basin, Australia

While searching topographic maps for potential impact structures, Shoemaker and Shoemaker (1985, 1986) selected for further studies an unnamed 9 km wide circle of inward-draining dry stream channels. This shallow basin is centered at 23°33' S, 124°45' E and lies near the transition zone between the Gibson and Great Sandy Deserts in Western Australia. The entire region is a broad plain of flat-lying sediments, armored with a residual sheet of laterite gravels and is lightly overprinted with a gentle pattern of dendritic paleodrainage. To workers in the field, the basin and its features are remarkably obscure. An inner bowl of flat sediments is ringed by a gentle, laterite-mantled topographic rim which is breached along its southwest margin. Inner rim slopes and the central basin floor are covered almost entirely by younger colluvium/alluvium deposits, dry lakebeds, and desert vegetation. Bedrock exposures are scattered and sparse, but repeated ground expeditions (summarized in Shoemaker and Shoemaker, 1989; Shoemaker *et al.*, 2001) have mapped the structure in detail. It is now formally named Connolly Basin and is an accepted terrestrial

FIG. 19. SRL L-band HH image of the Spider structure showing a bright central dome within the inner region of bright imbricated thrust sheets and surrounded by a darker halo of sediments covering the annular structural depression. Outermost faults and folds, as mapped by detailed fieldwork (E. M. Shoemaker, pers. comm., 1995) are not readily seen in radar images (SRL-1, DT 31.50; ASU photograph 4223-H).

impact structure. At the center of the structure, the oldest target rocks occur in an uplifted ring of steeply tilted, crushed, and shattered Permian sandstones that form a gentle mound ~1 km wide. Residual masses of a younger and intact Cretaceous-to-Tertiary marine sandstone, which occur in a discontinuous band circling the central uplift and in isolated blocks along inner rim slopes, are interpreted as erosional remnants of post impact crater filling sediments (Fig. 20).

In contrast to its obscure appearance in the field, the Connolly Basin radar signature dominates the SRL images on the track line passing over its position (Fig. 21). The entire image consists of a background of radar-gray matting due to the lack of significant surface slope effects and to an evenly distributed lateritic gravel surface. A broad network of ancient river channels is arranged in a dendritic system characteristic of flat-lying clastic sedimentary basins. River thalwegs appear radar bright due to roughness effects from surface, or near surface, riverbed gravels, and from electrical properties of evaporite salts concentrated from underlying strata (Veevers and Wells, 1959). Broad river banks appear soft edged and radar-dark, due to surface smoothing from accumulated silts and clays, and to transport of coarser sediments from surrounding lateritic plains into stream channels during rare periods of flowing surface waters. In radar, Connolly Basin

FIG. 20. E. M. Shoemaker kneels with a remnant block of crater-filling sandstone, now stranded on present Connolly Basin floor. Distant horizon is the slightly elevated rim of this very shallow and nearly featureless, exhumed structure (photograph courtesy of C. S. Shoemaker).

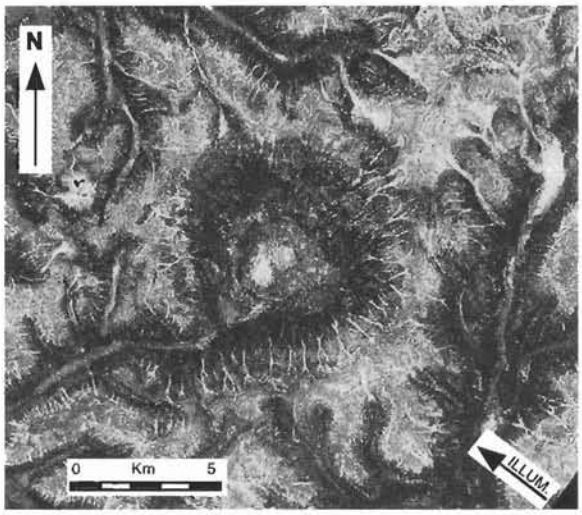

FIG. 21. SRL L-band HV image (DT-117.51) of Connolly Basin, Western Australia. Subtle and obscure in the field, this crater is quite prominent on radar imagery. Dark circular area comprises inner walls and floor where a bright playa lake lies next to the 1 km diameter central uplift ring of fractured sandstones.

prominently appears as a distinct, solitary radar-dark disk which interrupts regional textures (Fig. 21). Compared to the surrounding area, radar returns within the basin are reduced because of the absence of rough laterites and from signal attenuation by fine-grained sediments derived from post-impact fill. A radar-bright, salt-rich playa bed is clearly outlined adjacent to the slightly radar-darker ring of shattered central uplift rocks. A broad central zone of radar-mottled returns marks the flat crater floor, and the partial circle of remnant sandstone blocks is clearly imaged. In addition, the radial system of shallow gullies along the basin inner walls is distinctly imaged as a series of short bright lines. In effect, all significant surface and near-surface geologic elements of the otherwise subtly obscure Connolly Basin impact structure can be identified and located from a single SRL image.

Henbury Craters, Australia

Henbury consists of a group of small craters clustered at 24°35' S, 133°9' E in the central part of the Amadeus Basin, Northern Territory, Australia (Alderman, 1932). The crater field resulted from the impact of a swarm of iron meteorites and includes at least 13 craters ranging in size from 6 to 150 m in diameter. All are formed in shales, siltstones, and some sandstones of Precambrian age (Cook, 1968; Milton, 1968). The impact event is estimated to have occurred 4700 years ago based on carbon 14 dating (Shoemaker *et al.*, 1990).

Despite their small individual sizes, the three largest craters are overlapped and/or are adjacent (Bevan, 1996). As a result, their combined location within the Henbury field can be distinguished clearly in SRL imagery (Fig. 22). The crater cluster appears as a distinct, radar-bright mass embedded within a zone of radar-darker soils. Their distinct radar signatures result from a combination of impact-disrupted sedimentary rocks, dielectric properties of soils that contain both a significant meteoritic iron content (Hodge and Wright, 1971) and evaporite salts, and the influence of localized vegetation. Radar energy returning from the remaining smaller craters is lost among strong signals scattering from the narrow, east-west trending belt of Bacon Ridge sandstone.

SUMMARY

The 10 impact craters or impact-related features described here are visible on SRL images and, in many cases, are better seen than in aerial photographs. This is partly a consequence of the study that focused on impact craters in aeolian terrains. In these areas, thin sand deposits mantle parts of the impact structures. Comparison with optical images shows that the radar energy, particularly in the longer wavelengths, penetrates some of the sand mantles to reveal structures that are otherwise hidden from view. This enables not only a better estimate of the crater diameter but also a better definition of associated features, including ejecta deposits, fracture zones, and radial joints resulting from the impact.

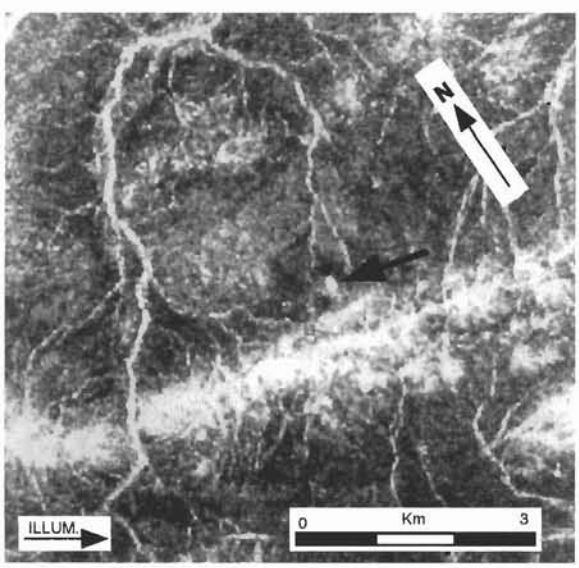

FIG. 22. SRL L-band HH image showing Henbury crater field. Visible are the three largest craters (arrow) which appear as a single radar-bright area. Radar is returned from evaporite salts, vegetation, and debris within their central depressions. The bright band crossing the image is an uplifted fault scarp known as Bacon Ridge (SRL-2, DT-21.80; ASU photograph 4221-H).

Thick sand deposits tend to result in low radar backscatter. Consequently, sand that has accumulated in topographically low areas often appears as radar-dark, enhancing topographic features resulting from the impact. Similarly, dry playa deposits, as in the Amguid crater floor, enhance the visibility of craters because of their low radar backscatter. In contrast, the central playas at Wolf Creek, Connolly Basin, and Henbury contain significant amounts of mineral salts (gypsum) and vegetation, which produce distinctly brighter radar signals.

Radar backscatter is sensitive to a wide variety of parameters, including soil moisture, vegetation, submeter-scale roughness, and the presence of boulders. Consequently, stream patterns often are enhanced in radar images compared to other forms of remote sensing. The development of stream patterns on impact structures often is controlled by slopes radiating from the crater rim and by radial and concentric fracture patterns. Thus, as demonstrated at the Zhamanshin feature, elements of an impact structure may be recognized by analyses of stream patterns.

The impact features imaged during the SIR-C/X-SAR missions occur in a range of environments that include all grades of vegetation and climates. These impact events also encompassed a variety of target materials, impact velocities, projectile compositions, and post-impact histories. Therefore, there is no single set of radar parameters (wavelength, incidence angle, or polarization) that is optimal for radar observation of terrestrial impact structures. Generally, however, longer wavelengths penetrate deeper to return radar signals from crater ejecta that might be obscured by aeolian materials. Also, images acquired at higher incidence angles (closer to horizontal) enhance topographic features such as crater walls.

Acknowledgments–This work was supported by the National Aeronautics and Space Administration through the Shuttle Imaging Radar-C project, Jet Propulsion Laboratory and the Planetary Geoscience Program. It has benefited from generous sharing of knowledge and information from D. Roddy, C. Shoemaker, and J. R. Underwood. We thank E. Turtle for a helpful review of the manuscript. We also thank D. Ball for photographic support, B. Erwin for word processing, and S. Selkirk for drafting.

Editorial handling: E. Asphaug

REFERENCES

ALDERMAN A. R. (1932) The meteorite craters at Henbury, Central Australia. *Mineral. Mag.* **23**, 19–32.

BECQ-GIRAUDON J. F., ROUZEAU O., GOACHET E. AND SOLAGES S. (1992) Impact hyperveloce d'une meteorite geante a l'origine de la depression circulaire d'Aorounga au Tchad (Afrique). *Comptes Rendus de l'Academie des Sciences, Ser. 2* **315**, 83–88.

BEVAN A. W. R. (1996) Australian crater-forming meteorites. *AGSO J. Australian Geol. Geophys.* **16**, 421–430.

COOK P. J. (1968) *Geological Series–Explanatory Notes, Henbury, N.T., Sheet SG/53-1, 1:250,000.* Bureau of Mineral Resources, Geology and Geophysics, Canberra, Australia. 19 pp.

DIETZ R. S. (1965) Roter Kamm, Southwest Africa: Probable meteorite crater. *Meteoritics* **2**, 311–313.

DIETZ R. S. AND MCHONE J. F. (1979) Volcanic landforms and astroblemes. In *Apollo Soyuz Test Project Summary Science Report*, vol. 2 (eds F. El-Baz and D. M. Warner), pp. 183–192. NASA SP-412, U.S. Govt. Printing Office, Washington, D.C., USA.

ELACHI C. *ET AL.* (1982) Use of the space shuttle for remote sensing research: Recent results and future prospects. *Science* **218**, 993–1003.

EL-BAZ F. AND BAHAY I. (1982) Crater forms in the Uweinat Region. In *Desert Landforms of Southwest Egypt: A Basis for Comparison with Mars* (eds. F. El-Baz and T. A. Maxwell), pp. 79–89. NASA CR-3611, U.S. Govt. Printing Office, Washington, D.C., USA.

FLORENSKY P. V. AND DABIZHA A. I. (1980) *Meteoritnyy Krater Zhamanshin.* Nauka Press, Moscow, Russia. 127 pp.

FRENCH B., UNDERWOOD J. R. AND FISK E. P. (1974) Shock metamorphic features in two meteorite impact structures, southeastern Libya. *Bull. Geol. Soc. Am.* **85**, 1425–1428.

FUDALI R. F. (1973) Roter Kamm: Evidence for an impact origin. *Meteoritics* **8**, 245–257.

GARVIN J. B. AND SCHNETZLER C. C. (1994) The Zhamanshin impact feature: A new class of complex crater? In *Large Meteorite Impacts and Planetary Evolution* (eds. B. O. Dressler, R. A. F. Grieve and V. L. Sharpton), pp. 249–257. GSA Special Paper **293**, Geol. Soc. America, Boulder, Colorado, USA.

GREELEY R., IVERSEN J. D., POLLACK J. B., UDOVICH N. AND WHITE B. (1974) Wind tunnel studies of Martian aeolian processes. *Proc. R. Soc. London* **341**, 331–360.

GREELEY R. *ET AL.* (1992) Aeolian features on Venus: Preliminary Magellan results. *J. Geophys. Res.* **97**, 13 319–13 345.

GREELEY R., SCHUBERT G., LIMONADI D., BENDER K. C., NEWMAN W. I., THOMAS P. E., WEITZ C. M. AND WALL S. D. (1994) Wind streaks on Venus: Clues to atmospheric circulation. *Science* **263**, 358–361.

GRIEVE R. A. F. AND SHOEMAKER E. M. (1994) The record of past impacts on Earth. In *Hazards Due to Comets and Asteroids* (ed. T. Gehrels), pp. 417–462. Univ. Arizona Press, Tucson, Arizona, USA.

GRIEVE R. A. F. AND THERRIAULT A. M. (1995) PDFS in quartz: Target effects (abstract). *Lunar Planet. Sci.* **26**, 515–516.

GRIEVE R. A. F., WOOD C. A., GARVIN J. B., MCLAUGHLIN G. AND MCHONE J. F. (1988) *Astronaut's Guide to Terrestrial Impact Craters.* LPI Technical Report **88-03**, Lunar and Planetary Institute, Houston, Texas, USA. 89 pp.

GRIEVE R. A. F., RUPERT J., SMITH J. AND THERRIAULT A. (1995) The record of terrestrial impact cratering. *GSA Today* **5**, 194–196.

GUPPY D. J. AND MATHESON R. S. (1950) Wolf Creek Meteorite Crater, Western Australia. *J. Geol.* **58**, 30–36.

HARMS J. E., MILTON D. J., FERGUSON J., GILBERT D. J., HARRIS W. K. AND GOLEBY B. (1980) Goat Paddock cryptoexplosion crater, Western Australia. *Nature* **286**, 704–706.

HODGE P. (1994) *Meteorite Craters and Impact Structures of the Earth.* Cambridge Univ. Press, New York, New York, USA. 124 pp.

HODGE P. W. AND WRIGHT F. W. (1971) Meteoritic particles in the soil surrounding the Henbury Meteorite Craters. *J. Geophys. Res.* **76**, 3880–3895.

JORDAN R. L., HUNEYCUTT B. L. AND WERNER M. (1995) The SIR-C/X-SAR synthetic aperture radar system. *IEEE Trans. Geosci. Remote Sensing* **33**, 829–839.

KOEBERL C. (1994) African meteorite craters: Characteristics and geological importance. *J. African Earth Sciences* **18**, 263–295.

KOEBERL C., HARTUNG J. B., KUNK M. J., KLEIN J., MATSUDA J. I., NAGAO K., REIMOLD W. U. AND STOTZER D. (1993) The age of the Roter Kamm impact crater, Namibia: Constraints from ^{40}Ar-^{39}Ar, K-Ar, Rb-Sr, fission track, and ^{10}Be-^{26}Al studies. *Meteoritics* **28**, 204–212.

KOEBERL C., REIMOLD W. U., VINCENT P. M. AND BRANDT D. (1998) Aorounga and Gweni Fada impact structures, Chad, central Africa: Petrology and geochemistry of target rocks (abstract). *Lunar Planet Sci.* **29**, #1103, Lunar and Planetary Institute, Houston, Texas, USA (CD-ROM).

LAMBERT P., MCHONE J. F., DIETZ R. S. AND HOUFANI M. (1980) Impact and impact-like structures in Algeria, Part I, four bowl-shaped depressions. *Meteoritics* **15**, 157–179.

LEFRANC J. P. (1969) Reconnaissance du Cratere Meteoritique d'Amguid (Mouter, Sahara Central). *Comptes Rendus des Seances de l'Academie des Sciences, Ser. D* **268**, 900–902.

LOWMAN P. D., JR. (1968) *Geologic Orbital Photography: Experience from the Gemini Program.* NASA Report X-644-68-228, Goddard Space Flight Center, Greenbelt, Maryland, USA. 34 pp.

LOWMAN P. D., JR. AND TIEDEMAN H. A. (1971) *Terrain Photography from Gemini Spacecraft: Final Geologic Report.* NASA Report X-644-68-228, Goddard Space Flight Center, Greenbelt, Maryland, USA. 75 pp.

LOWMAN P. D., JR., MCDIVITT J. A. AND WHITE E. H. (1966) *Terrain Photography on the Gemini IV Mission: Preliminary Report.* NASA Report X-641-66-52, Goddard Space Flight Center, Greenbelt, Maryland, USA. 8 pp.

MAINGUET M. AND CALLOT Y. (1978) L'erg de Fachi-Bilma (Tchad-Niger): Contribution a la connaissance de la dynamique des ergs et des dunes des zones arides chaudes. *Service. de Documentation et de Cartographie Geophysiques, Edtns. Centre national de la recherche scientifique, Memoires et documents; nouv. ser.* **18**, 184 pp. Paris.

MARTIN A. J. (1969) Possible impact structure in Southern Cyrenaica, Libya. *Nature* **223**, 940–941.

MASAITIS V. L., BOIKO Y. A. AND IZOKH E. P. (1984) Zhamanshin impact crater (western Kazakhstan): Additional geological data. *Proc. Lunar Planet Sci. Conf.* **15th**, 515–516.

MCCALL G. J. H. (1965) Possible meteorite craters; Wolf Creek, Australia and analogs. *New York Acad. Sci. Annals* **123**, 970–998.

MCCAULEY J. F., GROLIER M. J. AND BREED C. S. (1977) *Yardangs of Peru and Other Desert Regions.* U.S. Department of the Interior, Geological Survey, Interagency Report: Astrogeology 81, USA. 177 pp.

MCCAULEY J. F., SCHABER G. G., BREED C. S., GROLIER M. J., HAYNES C. V., ISSAWI B., ELACHI C. AND BLOM R. (1982) Subsurface valleys and geoarcheology of the eastern Sahara revealed by shuttle radar. *Science* **218**, 1004–1019.

MILLER R. M. AND REIMOLD W. U. (1986) Deformation and shock deformation in rocks from the Roter Kamm Crater, SWA/Namibia (abstract). *Meteoritics* **21**, 456–458.

MILTON D. (1968) *Structural Geology of the Henbury Meteorite Craters, Northern Territory, Australia.* U.S. Geol. Surv. Prof. Paper 599–C, U.S. Gov't. Printing Office, Washington, D.C., USA. 17 pp.

REEVES F. AND CHALMERS R. O. (1949) The Wolf Creek Crater. *Australian J. Sci.* **11**, 154–156.

REIMOLD W. U. AND MILLER R. M. (1989) The Roter Kamm impact crater, SWA/Namibia. *Proc. Lunar Planet. Sci. Conf.* **19th**, 711–732.

REIMOLD W. U., MILLER R. M., GRIEVE R. A. F. AND KOEBERL C. (1988) The Roter Kamm crater structure in SWA/Namibia (abstract). *Lunar Planet. Sci.* **19**, 972–973.

ROBERTS H. G. AND PERRY W. G. (1970) *Mount Elizabeth, Western Australia*, 1:250,000. Geological Series, Sheet SE/52-1, Map and Explanatory Notes, Bureau of Mineral Resources, Geological Survey of Western Australia, Australia. 16 pp.

ROLAND N. W. (1976) Die Ringstruktur Aorounga (Borkou, Sud-Sahara). *Geologisches Jahrbuch* **33**, 117–131.

SHOEMAKER E. M. AND SHOEMAKER C. S. (1985) Impact structures of Australia (abstract). *Meteoritics* **20**, 754–756.

SHOEMAKER E. M. AND SHOEMAKER C. S. (1986) Connolly Basin, a probable eroded impact structure in Western Australia (abstract). *Lunar Planet Sci.* **17**, 797–798.

SHOEMAKER E. M. AND SHOEMAKER C. S. (1988) The Spider Impact Structure, Western Australia (abstract). *Absts. w. Progs., Geol. Soc. Am.* **20**, 147.

SHOEMAKER E. M. AND SHOEMAKER C. S. (1989) Geology of the Connolly Basin impact structure, Western Australia (abstract). *Lunar Planet Sci.* **20**, 1008–1009.

SHOEMAKER E. M. AND SHOEMAKER C. S. (1996) The Proterozoic impact record of Australia. *AGSO J. Australian Geol. Geophys.* **16**, 379–398.

SHOEMAKER E. M. *ET AL.* (1990) Ages of Australian impact craters (abstract). *Meteoritics* **25**, 409.

SHOEMAKER E. M., PLESCIA J. B. AND SHOEMAKER C. S. (2001) Connolly Basin impact structure, Western Australia (abstract). *Lunar Planet Sci.* **32**, #1311, Lunar and Planetary Institute, Houston, Texas, USA (CD-ROM).

STOFAN E. R., EVANS D. L., SCHMULLIUS C., HOLT B., PLAUT J. J., VAN ZYL J., WALL S. D. AND WAY J. (1995) Overview of results of Spaceborne Imaging Radar-C, X-band Synthetic Aperture Radar (SIR-C/X-SAR). *IEEE Trans. Geosci. Remote Sensing* **33**, 817–828.

UNDERWOOD J. R., JR. (1976) Impact structures of the Libyan Sahara: Some comparisons with Mars. *Geologica Romana* **15**, 337–340.

VEEVERS J. J. AND WELLS A. T. (1959) Probable salt dome at Woolnough Hills, Canning Basin, Western Australia. *Australian J. Sci.* **21**, 193–195.